BogieBot: A Climbing Robot in Cluttered Confined Space of Bogies with Ferrous Metal Surfaces

Mohammad Adinehvand[1], Ehsan Asadi[1], Chow Y. Lai[2], Hamid Khayyam[1], Kevin Tan[3], Reza Hoseinnezhad[1]

***Abstract*— Proactive inspection is essential for prediction and prevention of rolling stock component failures. The conventional process for inspecting bogies under trains presents significant challenges for inspectors who need to visually check the tight and cluttered environment. We propose a miniature multi-link climbing robot, called BogieBot, that can be deployed inside the undercarriage areas of trains and other large vehicles for inspection and maintenance purposes, for the first time. BogieBot can carry a visual sensor or manipulator on its main body. The novel compact design utilises six identical couple joints and two mechanically switchable magnetic grippers that together, empower multi-modal climbing and manipulation. The proposed mechanism is kinematically redundant, allowing the robot to perform self-motions in a tight space and manoeuvre around obstacles. The mechanism design and various analyses on the forward and inverse kinematic, work-space, and self-motions of BogieBot are presented. The robot is demonstrated to perform challenging navigation tasks in different scenarios involving simulated complex environments.**

I. Introduction

As the rolling stock industry transitions to adopt condition-based maintenance, proactive fault detection is becoming increasingly in demand. Despite the recent advancements in robotics, no automated technology is yet available for inspecting components inside confined spaces in the under-carriage of railway vehicles (e.g. inside bogies). There are only two limited technologies used in this sector for inspecting external parts underneath the trains. Inside a bogie, the environment is very tight, consisting of various mechanical components. The need for pit to access underneath bogie and labour costs are the main concerns in the rolling stock inspection task. The manual inspection challenges motivate the need to design a robot that climbs freely inside the bogie and scans components for inspection.

Concerning the complex bogie environment, with surface transitions, irregularities and discontinuities, a number of challenges are encountered and should be considered in designing a robotic solution. A compact mechanism is required with flexibility and adaptability to change its shape for overcoming various obstacles. The most important factors in the design of such a robot are the locomotion type and adhesive technologies that allow the robot to move and climb in tight spaces. The existing robotic platforms can hardly meet all the above requirements. The related robots are reviewed in the next section considering three locomotion types: continuous, step-by-step, and hybrid locomotion.

[1]M. Adinehvand, E. Asadi, H. Khayyam and R. Hoseinnezhad are with School of Engineering, RMIT University, Melbourne, Australia
[2]C. Y. Lai is with University College London, United Kingdom
[3]K. Tan is with Downer Group, Melbourne, Australia.

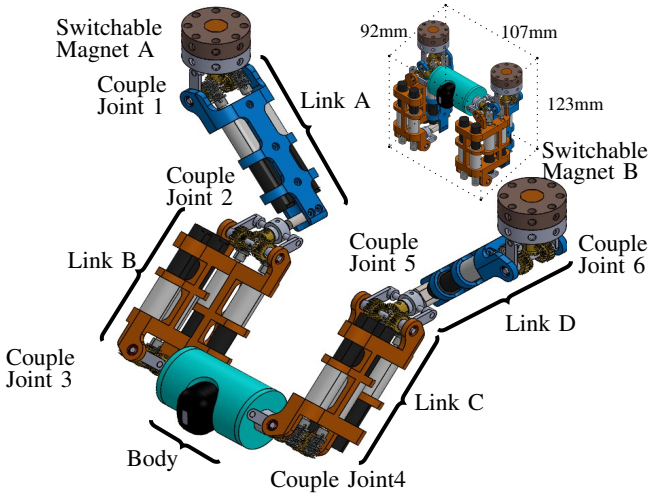

Fig. 1: The 3D schematics of the BogieBot design with six 2-DOF couple joints. One DOF of joints 1 & 6 on last links are connected to magnets to mechanically turn them on and off. The sensor is mounted on the body part and one DOF of joints 3 & 4 are used to rotate sensor 360°.

For the first time, a multi-modal climbing and manipulation robot, called BogieBot, is designed and modelled particularly to meet the needs of robotic inspection and maintenance of bogies in rolling stock. The robotic system is a redundant chain-link mechanism with six 2-DOF couple joints. It comes with four main links, and an inner body link to carry a visual sensor (e.g. a camera or scanner) or a manipulation tool. The first and last links are interconnected to two mechanically switchable magnetic grippers. Some key design features are:

1) The slim and compact mechanism is realized by the design of 2-DOF couple joints with differential gears and embedded motors inside the body link.
2) The robot's self-motion and flexibility are achieved through a kinematically redundant mechanism. It allows optimizing robot behaviour to perform secondary tasks such as obstacle and singularity avoidance,
3) The design allows switching between locomotion and manipulation modes or performing both concurrently. The robot can crawl or climb on ferrous material surfaces to move between components. It can also adjust its sensor position in manipulation mode to optimize the sensor's location for data acquisition,
4) By modular integration of additional couple joints and links, the robot reachability could be extended for operation in a larger environment than Bogie.

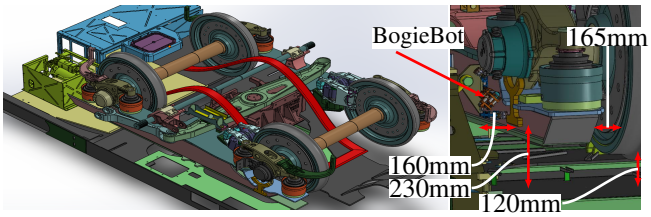

Fig. 2: Section view of a bogie. The robot needs to crawl into inaccessible locations (dimensions are rounded).

The rest of the paper is organised as follows. Section II presents the related works in this domain. In section III, the mechanical design of the robot is presented along with how it is actuated. Robot kinematics and its self-motion are then analysed in section IV followed by the description and results of simulation experiments which are presented in section V. Section VI concludes the paper.

II. Related Works

BogieBot is required to crawl into the inaccessible and tight environment in a 3-Dimensional space–see Fig. 2. Here, locomotion type of the robot and its ability to overcome gravity force play a vital role. The most popular locomotion types for climbing robots are continuous, step-by-step, and hybrid locomotion [1]. They employ different adhesive technologies, including magnetic force, mechanical, pneumatic, and electrostatic adhesion to overcome gravity force.

Continuous-motion robots, such as wheeled robots, generally offer fast and simple movements for inspection. However, dealing with obstacles is their main weakness.

Cy-mag^{3D} [2] is one of the tiniest magnetic wheeled robots that performs locomotion transitions in all directions from one surface to another at angles between $0°$ and $180°$ regardless of gravity. However, it cannot overcome irregularities, discontinuities, and obstacles due to its simple rolling structure and non-articulated chassis.

MagneBike [3] is also one of the well-known magnetic articulated wheeled robots. It can perform convex and concave locomotion transitions only up to $90°$ angles, but it has limited flexibility in tight spaces.

Tracked mobile robots offer stability. Combot [4] is a tracked robot with magnetic adhesion that can overcome up to 30 mm diameter obstacle on vertical surfaces. However, it has difficulty dealing with surface transition and more than $90°$ locomotion transitions.

Robots with step-by-step locomotion are also deployed in structural climbing. They use grippers interconnected through a chain-like mechanism. Legged robots have suitable mobility for applications in both structured and unstructured environments. However, in wall-climbing applications, their control strategies are relatively complicated [5].

Biped wall climbing robots, like [6, 7], have also shown ability to overcome obstacles. From size perspective, the former robot is bulky and not adaptable to tight spaces, and the later does not have enough DoF to to travel inside tight and confined space with large number of irregular obstacles. To make small robots faster, Brachiation locomotion is preferred through step-by-step swinging of the main body like a monkey or a pendulum [8]. Continuous Contact Brachiation [9] and Ricochetal Brachiation [10] have a great flexibility to jump from one place to another. This kind of locomotion is not applicable to the intended application, due to the lack of space for the take-off phase and the difficulty of switching phases. Moreover, undulatory locomotion is effective in the complex environment [11]. However, the capability of these mechanisms to mimic real wave shape is limited by the material's property. A soft structure, such as [12] allows flexible motions at the expense of control complexity corresponding to mechanism deformations [13].

Hybrid robots attempt to take advantage of both continuous and step-by-step movements such as speed and obstacle overcoming, respectively. However, existing hybrid robots do not not offer greater flexibility. For instance, OmniClimber [14] is a well-developed example, in which an articulated arm, as a climbing mechanism, is integrated with an omnidirectional mobile base to move faster on flat surfaces. However, although OmniClimber is a hybrid robot, it is merely able to overcome obstacles and plane transition.

Considering the pros and cons of the above robotic mechanisms, they can hardly meet all the requirements for moving freely inside the train bogies. Nature-inspired step-by-step robots such as [15, 16] are more capable to adapt and navigate around obstacles compared with continuous robots. However, the inflexibility and complexity of controlling their behaviour are the main shortcomings.

III. Mechanical Design and Actuation

With the goal of inspection and maintenance in rolling stock (e.g. bogies), a novel multi-modal climbing and manipulation robot, called BogieBot, is presented – see Fig. 1. It is designed with six couple joints, four main links, an inner body link (to carry a camera or a tool) and two mechanically switchable magnetic grippers. The robot design is unique in utilising six couple joints, and its compactness, flexibility and adaptability to move inside tight environments with ferrous surfaces. The size of the robot is $92mm \times 123mm \times 136mm$ at off configuration, and it can be extended to $482mm$ long.

BogieBot can perform climbing (or walking) tasks in two steps: chain-link movement and gripper switching. The robot can also rotate or move its main body, which is equipped with a sensor (as shown in Fig. 1) or a tool, to scan the surroundings in 360 degrees, or from a certain distance.

A. Couple Joints and Actuation System

To shape a compact actuation mechanism and to reduce the size of the BogieBot, we devised a 2 DOF couple joint with intersecting axes, as illustrated in Fig. 3. In total, the actuation system includes six couple joints which make twelve independent joints. Each couple joint consists of two brushless DC motors with encoders, two worm and wheel gears (with the ratio of 20:1), and three bevel gears.

The couple joint generates two DOF motions about q_{i1} and q_{i2} axes (Fig. 3) via controlling the speed and direction

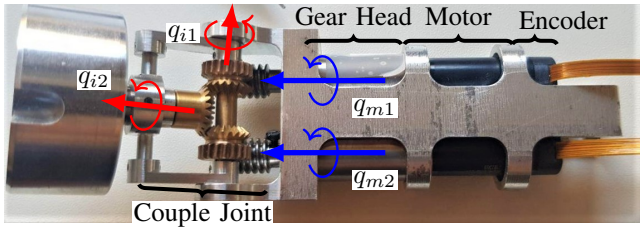

Fig. 3: 2-DOF couple joint with differential gear and embedded motors inside the link body. The resulting motion is a combination of rotation about two axes q_{i1} and q_{i2}.

of worms rotation about (q_{m1} and q_{m2}) axes. Assuming rigid transmission with no backlash, the relationship between input and output velocities (motor & joint speeds) is expressed as:

$$\dot{q}_{i1} = k_g(\dot{q}_{m1} + \dot{q}_{m2})/2, \dot{q}_{j2} = k_g(\dot{q}_{m1} - \dot{q}_{m2})/2 \qquad (1)$$

where k_g is gear ratio (1:20). According to (1), the output shaft solely revolves around the q_{i1} axis, when two gears are rotated at the same direction and speed. The whole system could also purely revolve around q_{i2} axis when worm gears are rotated in the opposite direction but at the same speed. The rotation around q_{i2} is used to turn on and off the magnet or rotate the attached link. The couple joint is using the power of both motors under certain circumstances.

B. Switchable Magnetic Gripper (SMG)

Using magnets as an adhesive technology is common in robots that need to climb surfaces. With this solution, energy consumption must be taken into consideration. We have employed a mechanically switchable magnetic gripper as depicted in Fig. 4, to reduce the power requirements. The proposed gripper governs ferromagnetic attraction forces by changing the magnetic flux paths. It consists of bottom and top holders. The top holder is fixed, and the bottom holder is driven via the main shaft and rotates relative to the top holder. Each holder is equipped with eight magnets. Magnets are mounted perpendicularly to the shaft in one side and small rods in the other side. The magnets are placed in opposite polarization directions by one interval. The gripper is activated once magnets of both holders are parallel with the same polarization direction. This way, the magnetic fluxes are circulated between rods and surface, and the attraction force is governed. Once the bottom holder is rotated by $45°$, the magnetic fluxes are internally circulated through magnets and rods, and adhesion forces are cancelled. Each gripper consists of 16 magnets with magnet force of 0.6kg per each. Considering the lowest coefficient friction of 0.3, each gripper can prevent 94.17N normal force and 28.25N shear forces. These value are significantly more than critical values depicted in TableI.

C. Multi-Modal Climbing and Manipulation

For the purpose of comprehensive inspection of the inside of the constrained Bogie space, the BogieBot should climb surfaces of complex shape and manipulate its sensor's

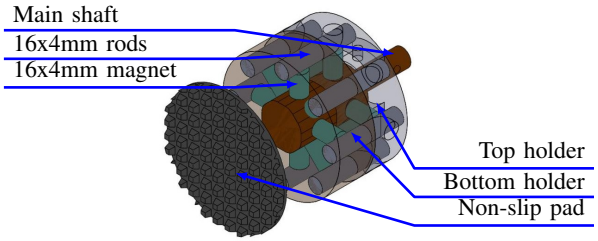

Fig. 4: Switchable magnet gripper; shaft and bottom holder are inter-connected. A 45° rotation of shaft will change the direction of magnetic flux and cancel adhesion force.

TABLE I: Normal and shear forces in the critical cases based on Newton-Euler recursive algorithm

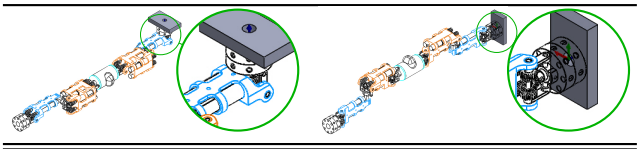

location to scan various parts. Climbing is performed via the sequence of motions shown in Fig. 5. Before and after each motion, both endpoints are fixed to the environment by means of grippers (Fig. 5.A). Then, one endpoint of the BogieBot is detached from the environment and moved in the three-dimensional space then fixed to a different location in the environment (Fig. 5.B). The motion continues by disconnecting the second endpoint of the BogieBot (Fig. 5.C), and moving it to another place (Fig. 5.D).

Two distinguishable configurations can be considered for the robot: open-chain and closed-chain configurations. The BogieBot behaves as an open-chain serial mechanism when only one endpoint is fixed to the environment. The mechanism with twelve joints is kinematically redundant empowering versatility and dexterity. This allows self-motion of six degree-of-redundancy to achieve secondary behaviours and move over surfaces of complex shape via changing BogieBot's body shape. A closed-chain configuration is formed by attaching both ends to the environment. In this configuration, BogieBot can manipulate the embedded sensors mounted on its body link. For instance, it can scan the bogie by moving the sensor along a desired path and angle.

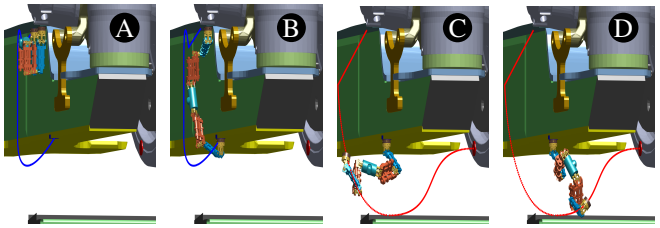

Fig. 5: Simulated model of BogieBot climbing inside a Bogie. A: initially both robot's ends are gripped to the bogie. B: first end is released, moved and gripped it to next point (blue path). C: the second end is released. D: the second end is moved toward the goal (red path).

IV. Kinematic and Self-Motion Analysis

Six degrees of freedom redundancy allows the robot to execute a task with a wide range of possible motions (the so-called self-motion or internal motions). Such a feature plays a key role in climbing and moving in congested environments. Kinematic analysis of BogieBot is discussed in this section for both modes of motion, i.e. the climbing mode (open-chain) and manipulation mode (closed-chain). Importantly, we demonstrate how employing self-motions leads to avoiding singular configurations in the presence of actual joint limits and workspace obstructions.

A. Forward Kinematics

The forward kinematic governs a nonlinear mapping from the joint space to the task space as follows:

$$x(t) = f\left(q(t)\right) \tag{2}$$

where x and q are vectors of end-link pose and joint angles, respectively. The relationship between velocity of end-link and robot joints is represented by Jacobian matrix:

$$\dot{x}(t) \coloneqq \begin{bmatrix} v(t) \\ \omega(t) \end{bmatrix} = J(q)\dot{q}(t) \tag{3}$$

where J is called geometrical Jacobian matrix of the system and v and ω are linear and angular velocities, respectively. Having forward kinematics, one can use direct differentiation (for linear Jacobian), iterative methods (e.g. velocity propagation) or an explicit form to calculate Jacobian. However, the solutions of direct kinematics for open-chain (climbing) and closed-chain (manipulation) modes of BogieBot are not identical, as the primary task in each mode is different.

1) Climbing mode (open-chain): The main task in climbing is to move one endpoint of the robot at a desired path. Hence, the direct kinematic is expressed by the pose of BogieBot's free end-link $x(t) = [X\ Y\ Z\ \theta\ \phi\ \psi]^\top \in \mathbb{R}^6$ with respect to its fixed end, as a function of joint angles $q(t) \in \mathbb{R}^{12}$. This way, the kinematic equation is represented by a homogeneous transformation matrix, $\mathbf{T}$.

$$^{fixedSMG}\mathbf{T}_{freeSMG} = \prod_{j=1}^{j=12} {}^{j-1}\mathbf{T}_j = f(q), \tag{4}$$

TABLE II: Mechanical Properties

DH Parameters											
Link	a_i	α_i	d_i	q_i	q_{lim}	**Link**	a_i	α_i	d_i	q_i	q_{lim}
1	0	0°	10	q_{11}	-180:180	2	0	-90°	28.5	q_{12}	-50:185
3	79.46	0°	0	q_{21}	-180:180	4	0	90°	37	q_{22}	-170:40
5	76	-90°	2	q_{31}	-55:145	6	0	90°	-18	q_{32}	-180:180
7	0	0°	47.5	q_{41}	-180:180	8	0	90°	47.5	q_{42}	-55:145
9	76	-90°	18	q_{51}	-10:170	10	0	90°	12	q_{52}	-180:180
11	79.46	0°	37	q_{61}	-90:140	12	0	90°	28.5	q_{62}	-180:180

Mass Properties				
Part	m(g)	Ix($g.mm^2$)	Iy($g.mm^2$)	Iz($g.mm^2$)
Link A&D	31.19	33.8e-2	194.3e-2	209.2e-2
Link B&C	52.22	161.7e-2	293.6e-2	380.6e-2
Couple Joints	.1e-2	5.3e-2	7e-2	10.9e-2
Body	121.55	210.9e-2	406e-2	433e-2

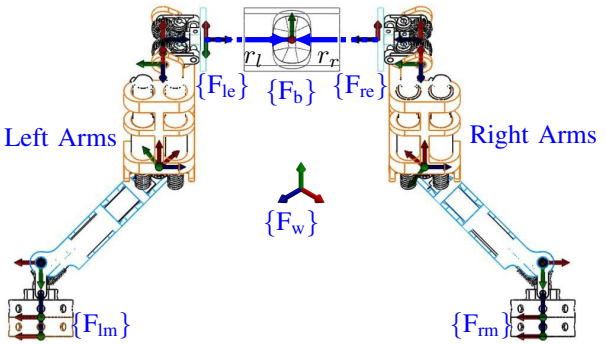

Fig. 6: Closed kinematic chain formed by fixing both ends of the robot. This model imposes some geometrical constraints.

where j indicates the joint number. Denavit and Hartenberg convention is used here to derive the transformation matrix by finding the DH parameters – see Table II.

2) Manipulation mode (closed-chain): It is required to control the pose of body-link (camera) in Cartesian space while both grippers are attached to the surface. To deal with this, BogieBot's mechanism is considered as double arms which manipulate its body in the presence of some constraints – see Fig. 6 (left chain: links A and B, right chain: links C and D). This way, forward kinematics is expressed by pose of the left and right end-effectors with respect to the left and right magnets, as a function of Arm's joint angles q_l or $q_r \in \mathbb{R}^6$, respectively. The kinematic equation for two open-chains are written as:

$$^{\gamma m}\mathbf{T}_{\gamma e} = \prod_{j=1}^{j=6} {}^{j-1}\mathbf{T}_j^l = f_\gamma(q), \tag{5}$$

where γ is l or r corresponding to left and right arms receptively, m and e correspond to the frames attached to magnets ($\{F_{lm}\}$ & $\{F_{rm}\}$) and frames attached to the end chain links ($\{F_{le}\}$ & $\{F_{re}\}$), respectively. As can be seen from Fig. 6, the pose of the end link of the right and left arms must satisfy the main body's pose based on the geometric relationship. This constraint can be formulated in terms of pose, velocity and acceleration. For a particular camera's pose $^w\mathbf{T}_b$, the kinematic constraint can be written as:

$$^w\mathbf{T}_b = \underbrace{{}^w\mathbf{T}_{lm}\,{}^{lm}\mathbf{T}_{le}\,{}^{le}\mathbf{T}_b}_{\text{via left arm}} = \underbrace{{}^w\mathbf{T}_{mr}\,{}^{rm}\mathbf{T}_{re}\,{}^{re}\mathbf{T}_b}_{\text{via right arm}} \tag{6}$$

where $^w\mathbf{T}_{lm}$ and $^w\mathbf{T}_{rm}$ depend on the previous phase of the movement. Assuming that BogieBot is fully attached to the surface, $^w\mathbf{T}_{ml}$ and $^w\mathbf{T}_{mr}$ are constant. The velocity constraint can be formulated as follows:

$$\dot{x}_b(t) = \begin{bmatrix} \mathbf{I} & -(r_r)^\times \\ \mathbf{0} & \mathbf{I} \end{bmatrix} \begin{bmatrix} v_{er}(t) \\ \omega_{er}(t) \end{bmatrix} = \begin{bmatrix} \mathbf{I} & -(r_l)^\times \\ \mathbf{0} & \mathbf{I} \end{bmatrix} \begin{bmatrix} v_{el}(t) \\ \omega_{el}(t) \end{bmatrix} \tag{7}$$

where r_r and r_l denote location of body frame w.r.t left and right arms' end-effector, –see Fig. 6.

B. Inverse Kinematic and Self Motions of Open-Chain

Inverse kinematics could be considered as a general damped optimisation problem to reach a continuous and feasible solution in the presence of singular points [17]. This general solution can be obtained by expressing the inverse kinematics problem as:

$$\min_{\dot{q}} \left\{ \|\dot{x} - J\dot{q}\|^2_{W_a} + \Lambda \|\dot{q} - q_{arb}\|^2_{W_f} \right\} \quad \text{subject to } \dot{x} = J\dot{q} \tag{8}$$

Where W_a and W_f are positive definite matrices, which are related to accuracy of tracking and feasibility of tracking in preventing joint velocity limits. Λ is a positive scalar chosen to compromise feasibility of joints velocity and tracking error respectively. q_{arb} is an arbitrary. A range of numerical methods such as LSM, and D-LSM lie in the above definition. For instance by considering, $\Lambda = \lambda^2$, $W_a = I$, and $W_f = I$, (8) yield to D-LSM method.

For a redundant system, with $m < n$, and for any predefined $\dot{x}$ may exist infinite $\dot{q}$ satisfying $\dot{x} = J\dot{q}$. Eventually, a singularity-robust IK can be obtained by:

$$\dot{q} = J^* \dot{x} + (I - J^* J)\, q_{arb} \tag{9}$$

where:

$$J^* = W_f^{-1} J^T \left(J W_f^{-1} J^T + \Lambda W_a^{-1} \right)^{-1} \tag{10}$$

and its elements of weighted matrix are defined

$$w_{ii_f} = \begin{cases} 1 + |\frac{\partial H(q)}{\partial q_i}|, & if \Delta |\frac{\partial H(t)}{\partial q_i}| \geq 0, \\ 1 & if \Delta |\frac{\partial H(t)}{\partial q_i}| < 0, \end{cases} \tag{11}$$

where:

$$H(q) = \sum_{i=1}^{n} = \frac{1}{4} \frac{(q_{imax} - q_{imin})^2}{(q_{imax} - q_i)(q_i - q_{imin})} \tag{12}$$

so when q_i approaches to its boundary, $\partial H(q)/\partial q_i \to \infty$, consequently i^{th} element of W_f^{-1} becomes zero and joint number i will be stopped. The first term of (9) is the particular inverse solution of (3) and its second term projects an arbitrary vector q_{arb} to the null space of J, $\mathcal{N}(J)$. This homogeneous solution does not contribute to gripper motion and provides a mathematical tool to handle *self-motion* of redundant manipulator. This way, the inverse kinematics and self-motions are solved using algorithm 1.

C. Workspace Analysis

The feasible workspace of BogieBot is calculated numerically and depicted in Fig. 7, by adopting the Gaussian Growth Monte Carlo method [18]. Assuming one end of the BogieBot is fixed to the environment and no joint constraints, the other end and embedded sensor should reach surfaces of two spheres with radius of $R = 48.2\ cm$ (grey) and $r = 24.1\ cm$ (light blue), respectively. However, due to joint limits, the feasible workspaces shrink to smaller spaces as indicated in Fig. 7. The cloud of points highlighted by dark blue and red colour are the estimations of feasible workspace due to joint limits. The feasible workspaces in the bottom semi-spheres reach closely to the maximum boundaries, due to ceiling mount of the gripper to the environment.

Algorithm 1: Inverse Kinematic

```
Initialise: ẋ_d, q_0 and q̇_max
for t_i ∈ [t_0, t_e] do
    Calculate J and σ_min(J);
    if σ_min(J) > 0 then
        J^(g) = VΣ^†U^T = J^T(JJ^T)^-1
    else
        switch Solver do
            case Optimal Λ do
                Solve ‖q̇^op‖²_Wf = ‖q̇_max‖²_Wf to find Λ^op
            case D-LSM do
                Constant Λ [19]
        J^(g) = W_f^-1 J^T (J W_f^-1 J^T + Λ W_a^-1)^-1
Return J^(g)
```

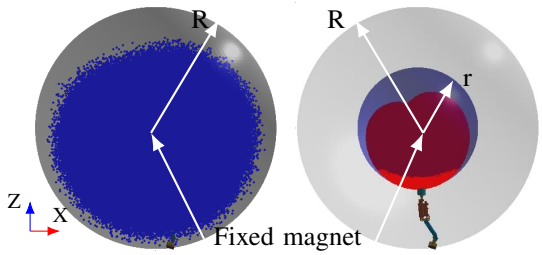

Fig. 7: Feasible workspaces. The cloud points in left image (blue points) and right image (red points) are estimations of the feasible workspace for BogiBot's free-end and its sensor, respectively. Imaginary maximum reachable spaces in the presence of no physical constraints are also indicated by grey and light-blue spheres, R and r, respectively.

V. Simulation Experiments and Results

Climbing in tight and narrow spaces and moving around obstacles are considered as the main requirement for inspection inside a bogie. The performance and ability of BogieBot to meet above requirements are evaluated by performing simulation experiments in the three challenging scenarios.

A. Controller Design

Torque controller can be expressed as [20]:

$$\tau_{act} = M(q)(\ddot{q}_d - K_d \dot{q}_e - K_p q_e) + C(q, \dot{q})\dot{q} + G(q) \tag{13}$$

where $q,\ \dot{q},\ \ddot{q} \in \mathbb{R}^{n\times 1}$ are the joint angles, angular velocity, and acceleration respectively. The calculation of inertia matrix $M(q) \in \mathbb{R}^{n\times n}$, Coriolis and centrifugal forces $C(q, \dot{q}) \in \mathbb{R}^{n\times n}$, where $e = q_d - q$ and $\dot{e} = \dot{q}_d - \dot{q}$ are the position and velocity joints error respectively. With this controller input, the system dynamics becomes a second-order ODE:

$$\ddot{e} + K_d \dot{e} + K_p e = 0, \tag{14}$$

Where, $K_d = 100I$ and $K_p = 20I$ are chosen.

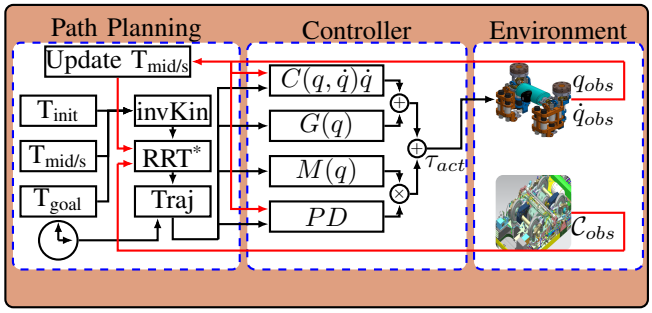

Fig. 8: The control block diagram of closed-loop system. **High-level strategy**: RRT* is used to generate desired paths in joint configuration. Initial, intermediate and goal locations of gripper, T_{init}, $T_{mid/s}$ and T_{goal}, are assumed to be known. Final configuration of each phase of movement is fed back to plan the next movement. **Low-level strategy**: A feedback linearization controller is employed to follow desired path.

B. Experiment Scenarios and Results

C. Path planning and collision avoidance

RRT* is employed in the experiments to address path planning problem. A feasible path in open-chain mode is restricted by intrinsic constraints of BogieBot (e.g. joint limits), and environmental constraints of Bogie (e.g. collision avoidance). BogieBot offers a freedom in the choice of configuration (e.g goal configuration) due to its self motions. Thus, a set of valid goal configuration is defined, using Workspace Goal Regions (WGRs) [21], which increases speed of finding the path. A WGRs consists of three parts:

- ${}^{0}\mathbf{T}_{w}$: transform from the origin to the WGR frame w,
- ${}^{w}\mathbf{T}_{e}$: end-effector offset in the coordinates of w,
- ${}^{w}\mathbf{B}$: 6×2 matrix of bounds in the coordinates of w.

where

$$ {}^{w}\mathbf{B} = \begin{bmatrix} \delta x_{max} & \delta y_{max} & 0 & 0 & 0 & \pi \\ \delta x_{min} & \delta y_{min} & 0 & 0 & 0 & -\pi \end{bmatrix}^{T} \quad (15) $$

where the first three columns and the last three ones bound the allowable translation and rotation, respectively, about x, y and z, in the w frame. $|\delta x| = |\delta y| = 1mm$ indicate the allowable position error along x and y, respectively.

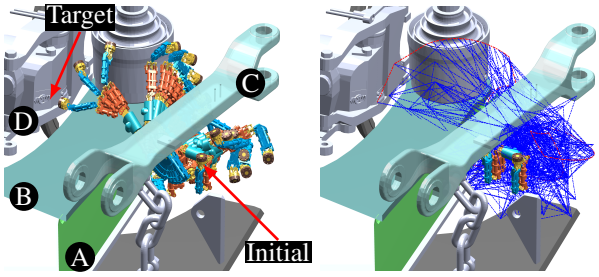

Fig. 9: Case Study 1: Direct Kinematics determine the pose of gripper in the Cartesian space (blue points) for each sample points in the $\mathcal{C}_{free}$. The valid path (red points) implicitly shows that $\mathcal{C}_{free}$ is connected and BogieBot can reach the target by crossing the narrow passage between A, B, and C.

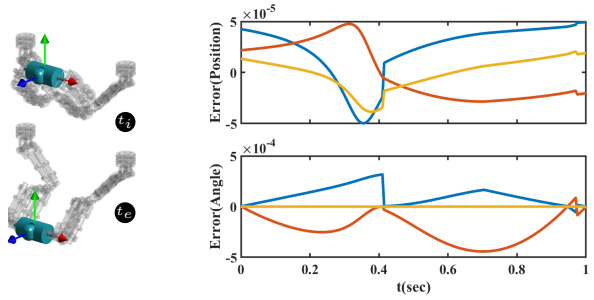

Fig. 10: Case Study 2 (Moving sensor along a desired path and orientation): Left plot shows the capability to move the body link without changing the direction of sensor view point in close chain mode. Right graph shows the location and angles error between left and right side of the robot represented by $\{F_{le}\}$ & $\{F_{re}\}$ frames, as shown in Fig 6.

1) Case 1: Connectivity of free space close to obstacles: Assuming that the robot's joint angle set and the surrounding obstacles are represented by $\mathcal{C}$ and $\mathcal{C}_{obs}$, respectively. By definition, the collision-free configuration space is simply computed as $\mathcal{C}_{free} = \mathcal{C} \backslash \mathcal{C}_{obs}$. Note that, cluttered $\mathcal{C}_{obs}$ could result in dividing the $\mathcal{C}_{free}$ into two or multiple disconnected free spaces, where finding a path between these spaces is impossible. To examine this, consider a complex situation, a narrow passage between parts A, B and C depicted in Fig. 9. RRT has been employed to directly sample joint angles in the$\mathcal{C}$-Space by 50% biased to target points. Direct Kinematics determine the pose of free magnet in the Cartesian space (blue points) for each collision free sample points. The results show that BogieBot is able to maintain its $\mathcal{C}_{free}$ connected via a valid path (red points) and crawl from C to D by passing into the narrow passage.

2) Case 2: Moving sensor along a desired path (closed-chain motion): BogieBot is able to rotate its sensor about its axis. It can also move its sensor along a desired path while both robot ends are connected to the surface. This closed chain configuration makes BogieBot more stable helping to acquire more accurate data. These closure constraints add extra limitations in finding a feasible path. Fig 10 shows the BogieBot in a ceiling mount configuration, while moving its sensor attached to the body link (highlighted in green). While the sensor is moved along x and y directions of its coordinate frame, the movement along z direction and yaw, pitch, and roll rotations are kept fixed. As can be seen from Fig 10, position errors (e_x, e_y, e_z) and Euler angle errors $(e_\theta, e_\phi, e_\psi)$ between right and left arms ends are negligible, $\mathcal{O}(10^{-5})$ and $\mathcal{O}(10^{-4})$, respectively.

3) Case 3: Sequence of movements in narrow spaces.: This experiment demonstrates the robot flexibility in crossing through narrow passages via sequences of motion. In the this scenario, the robot's task is to cross through a hole modeled by 4 horizontal blocks and then to climb up to a vertical block at the other side of the hole, as shown

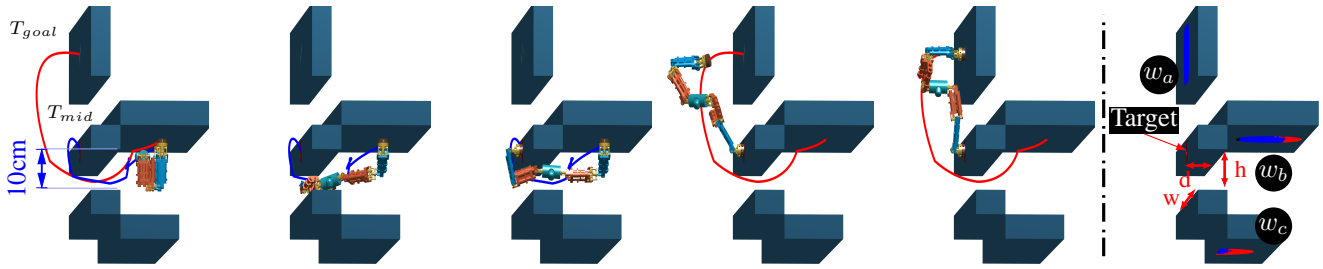

(a) Initial q. (b) Intermediate q. (c) Reach first point (d) Intermediate q. (e) Final q. (f) Adaptiveness Test

Fig. 11: Case Study 3 (simulated environment): (a)-(e) A sample of trials and sequence of multi-step motions in which BogieBot crossed through a hole (blue path) and then climbed vertically at the other side of the hole (red path).
(f): Robustness to initial position change: initial positions are distributed within 3 circles on different surfaces (w_a, w_b, w_c). Blue and red points differentiate initial points if the robot was able to reach target in single or multiple steps, respectively.

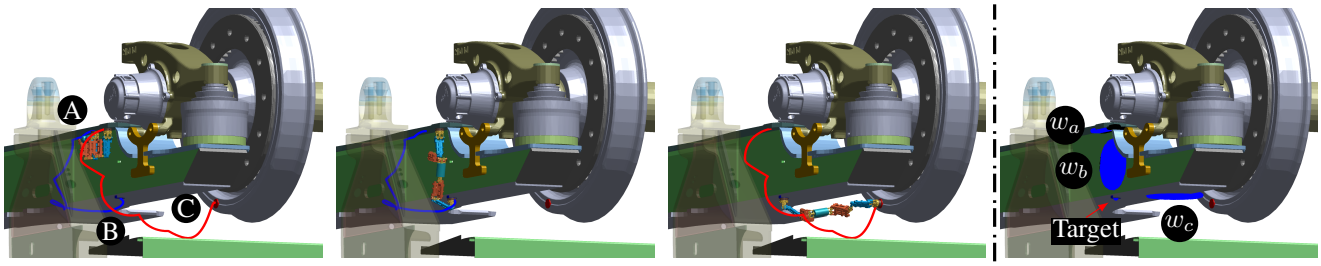

(a) Initial Configuration (b) Reach to the next point (c) Final Configuration (d) Adaptiveness Test

Fig. 12: Case Study 4 (Bogie environment): A trial sample (a) BogieBot is initially attached to part A, (b) then moved down its end to part B (b) and (c) finally moved the other end and gripped it to part C. Feasible paths by RRT are shown in blue (between part A and B) and red (between part A and C). (d): Robustness to initial position changes (w_a, w_b, w_c) .

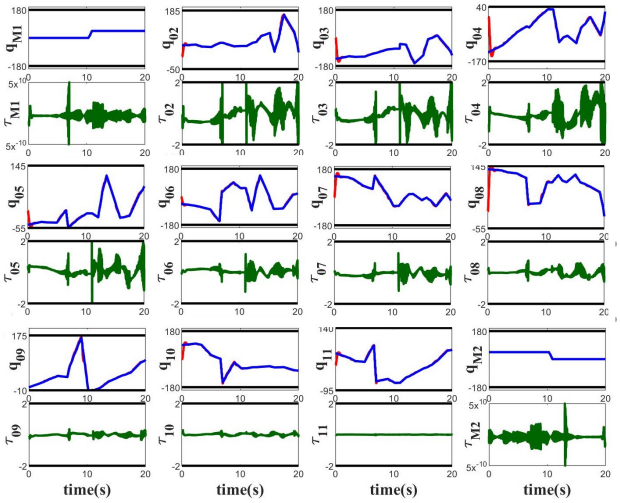

Fig. 13: Case Study 4 - Feedback Linearisation Controller. First, third and fifth rows indicate desired joint angles (blue), and actual joint angles (red). Second, forth and sixth rows indicate required torques (green), including their limits.

in Fig. 11. The feasible path is generated using RRT* in two steps from the initial configuration to an intermediate location (blue path) and subsequently to the final location (red path). Sequences of motion are shown in Fig. 11(a-e), in which BogieBot successfully followed the desired trajectories, passed the hole, overcame the obstacles, and climbed to the final position.

4) Case 4: Tightest spot of Bogie: This experiment is conducted around the hardest-to-reach spots of the bogie, which is depicted in the Fig. 12. The robot's task is to move down its end from part A to part B and then move the other end and attach it to part C. The feasible paths and resulted sequences of motion are shown in Fig. 12. In addition, the results of implemented controller for the last experiment is depicted in the Fig. 13. Apart from the beginning of motions, the results show small error between the achieved joint angles and the desired ones. Each joint is initialized at zero position (off configuration), that result in an initial error, but it vanishes within 1 sec.

5) Case 5: Adaptiveness to variations in the initial position and size of the narrow pathway: to evaluate the adaptiveness, trials were made with different starting locations and pathway sizes (h, w and d), Fig. 11f, using Monte Carlo simulation. The initial positions were distributed on three different horizontal and vertical surfaces. For each surface, 3000 initial positions are uniformly sampled within a circle of 10cm, and the simulation was performed for all feasible samples. Figs. 11f and 12d plots the starting configurations that were tried for environments in case 3 and 4. Samples are discarded if they are not lying on the environment's surface or there is a collision between robot and environment at

initial configuration. For example, the number of valid points on the w_a region in case 4 is 1218, as the surface on bogie is so tiny. More information about samples and results can be found in the Table. III and are summarised here.

For the majority of feasible initial positions in case 4, 99,9%, and relatively high rate of samples in case 3, 77.3% (w_a), 99,9% (w_b), and 25,4%(w_c), the robot is able to reach the target with less than 1mm error (blue samples). For the rest of feasible samples, the robot can reach the target in single-step with more than 1mm error, or in multi-steps with less than 1mm error (red samples). However, the simulations with different sizes of narrow pathways, Fig. 11f, show that the BogieBot is not able to navigate into holes with less than 10cm height, 8cm width and more than 14cm depth.

TABLE III: Adaptiveness result - Monte Carlo simulation

Case 3	Sample	Single Step	Case 4	Sample	Single Step
w_a	2912	77.3%	w_a	1218	99.9%
w_b	2439	99.9%	w_b	2985	99.9%
w_c	1581	25.4%	w_c	3000	99.9%

VI. Conclusion

Current practices for condition assessment of undercarriage vehicle are mostly manual. The need for a pit to access underneath a bogie is also a critical challenge. A miniature robot, called BogieBot, is proposed for automated inspection. The robot can climb inside a Bogie and manipulate position of its sensor for data acquisition. The robot mechanism design is unique in utilising six couple joints, and its flexibility and adaptability in performing locomotion and manipulation inside tight spaces with ferrous surfaces. Various analyses on the forward and inverse kinematic, workspace, and self-motions of BogieBot are presented. The robot is demonstrated to perform locomotion tasks in different complex scenarios involving simulated environments. The results indicate robot's flexibly and dexterity to perform self-motions in cluttered spaces and to cross through narrow passages via sequences of movement. Future work includes testing the robot prototype in actual field settings and deploy it inside a bogie. Reinforcement learning could be also applied for improving motion planning, controller optimization, and scenario-based learning policies inside a Bogie.

Acknowledgement

The authors greatly appreciate the financial support from the Rail Manufacturing Cooperative Research Centre (funded jointly by participating rail organisations, and the Australian Federal Government's Business Cooperative Research Centres Program) through Project R2.7.10.

References

[1] A. Peidró et al. "Design of compact switchable magnetic grippers for the HyReCRo structure-climbing robot". In: *Mechatronics* 59 (2019).

[2] F. Rochat et al. "Cy-mag3D: a simple and miniature climbing robot with advance mobility in ferromagnetic environment". In: *Ind Rob* (2011).

[3] F. Tâche et al. "MagneBike: Compact magnetic wheeled robot for power plant inspection". In: *1st CARPI* (2010).

[4] G. Lee et al. "High-payload climbing and transitioning by compliant locomotion with magnetic adhesion". In: *Rob Auton Syst* 60.10 (2012).

[5] W. Cheah et al. "Advanced motions for hexapods". In: *Int J Adv Robot Syst* 16.2 (2019).

[6] Y. Guan et al. "A modular biped wall-climbing robot with high mobility and manipulating function". In: *IEEE/ASME Trans. Mechatronics* 18.6 (2012).

[7] M. Minor et al. "Design, implementation, and evaluation of an under-actuated miniature biped climbing robot". In: *IROS* 3 (2000).

[8] C.-Y. Lin and Z.-H. Yang. "TRBR: Flight body posture compensation for transverse ricochetal brachiation robot". In: *Mechatronics* 65 (2020).

[9] H. Kajima et al. "Energy-based swing-back control for continuous brachiation of a multilocomotion robot". In: *Int. J. Intell. Syst.* 21.9 (2006).

[10] H. Cheng, C. Rui, and L. Hao. "Motion Planning for Ricochetal Brachiation Locomotion of Bio-primitive Robot". In: *IEEE-CYBER* (2017).

[11] R. Liu and Y.-a. Yao. "A novel serial–parallel hybrid worm-like robot with multi-mode undulatory locomotion". In: *Mech Mach Theory* 137 (2019).

[12] B. Gamus et al. "Understanding Inchworm Crawling for Soft-Robotics". In: *IEEE RA-L* 5.2 (2020).

[13] J. Cao et al. "Control of a soft inchworm robot with environment adaptation". In: *IRE Trans. Ind. Electron.* 67.5 (2019).

[14] M. Tavakoli et al. "The hybrid OmniClimber robot: wheel based climbing, arm based plane transition, and switchable magnet adhesion". In: *Mechatronics* 36 (2016).

[15] T. L. Lam and Y. Xu. "A flexible tree climbing robot: Treebot-design and implementation". In: *ICRA* (2011).

[16] I. H. Han et al. "A miniaturized wall-climbing segment robot inspired by caterpillar locomotion". In: *Bioinspir Biomim* 12.4 (2017).

[17] Y. Nakamura and H. Hanafusa. "Inverse kinematic solutions with singularity robustness for robot manipulator control". In: *J. Dyn. Sys., Meas., Control.* (1986).

[18] A. Peidró et al. "An improved Monte Carlo method based on Gaussian growth to calculate the workspace of robots". In: *Eng Appl Artif Intell* 64 (2017).

[19] T. Sugihara. "Solvability-unconcerned inverse kinematics by the Levenberg–Marquardt method". In: *IEEE Trans. Robot.* 27.5 (2011).

[20] F. L. Lewis, D. M. Dawson, and C. T. Abdallah. *Robot manipulator control: theory and practice*. CRC Press, 2003.

[21] D. Berenson et al. "Manipulation planning with workspace goal regions". In: *ICRA*. IEEE. 2009, pp. 618–624.